IEEE Access
Multidisciplinary | Rapid Review | Open Access Journal

Date of publication xxxx 00, 0000, date of current version xxxx 00, 0000.

Digital Object Identifier 10.1109/ACCESS.2017.DOI

Computer Simulation of Magnetoelectric Antenna and Performance Comparison with Micro-Loop

FAZEL RANGRIZ ROSTAMI[1], ALI KHALEGHI[1], (Senior Member, IEEE), and ILANGKO BALASINGHAM[1,2], (Senior Member, IEEE)

[1]Department of Electronic systems, Norwegian University of Science and Technology (NTNU), Trondheim 7491, Norway (e-mail: fazel.rangriz.rostami@ntnu.no)
[2]Oslo University Hospital (OUS), Oslo 0372, Norway

Corresponding author: Fazel Rangriz Rostami (e-mail: fazel.rangriz.rostami@ntnu.no).

This work was supported by the Research Council of Norway under the project of Wireless In-Body Sensor and Actuator Networks (WINNOW), Grant No. 270957.

ABSTRACT Electromagnetic radiation can be produced using functional materials such as magneto-electric (ME) composites, in which the magnetoelasticity and piezoelasticity of material are involved. The mechanical nature of the vibrations is used to miniaturize the ME antenna to micro-scale size. The antenna performance evaluation requires a multiphysics analysis of the structure. An ME antenna design and simulation is detailed using the finite element method (FEM) in COMSOL Multiphysics® in which the structural mechanics, electrostatics, and magnetic field physics are coupled together to address the simulation needs. An antenna size of 250 μm × 50 μm × 1 μm is simulated within a static magnetic bias field of 20 mT. The nonlinear isotropic model is used for magnetostrictive material definition in which the prestress is defined by the magnetic bias. The model is linearized for radio frequency (RF) simulations to account for the AC simulation. The antenna farfield radiation pattern and the gain are computed using finite difference time domain (FDTD) by incorporating the extracted nearfield of the ME antenna in COMSOL. The simulated antenna impedance, radiation pattern and antenna gain are compared to an equivalent micro-loop magnetic antenna. In addition, electromagnetic computations are used to evaluate the coupling performance between the ME antenna and a larger loop antenna over a distance up to 20 mm in free space and biomedical tissues to address the potential of using ME antenna in medical implants for wireless communication and wireless power transfer.

INDEX TERMS Biomedical implants, FEM method, magnetoelectric coupling, magnetoelectric antenna, near-field communications, nonlinear magnetostrictive.

I. INTRODUCTION

MINIATURIZATION of the antenna in sensors or wireless devices without performance degradation is of great importance. However, with conventional antennas such as dipoles and loops, the antenna efficiency will dramatically decrease when they are used in smaller electrical sizes i.e. ka < 0.1 where k is the wavenumber of free space and a is the radius of the sphere encircle the antenna [1]. On the other hand, small electrical size is more interesting in compact applications such as biomedical implants in which the space is limited and low-frequency operation is of great interest. Another problem with the miniaturization of conventional low-profile planer antennas is the current image that is created on the antenna ground plane that reduces antenna radiation efficiency, which is also known as the platform effect in the literature. To overcome this problem, instead of using a high dielectric material, one can use magneto-dielectric substrates [2], [3]. However, in the magneto-dielectric material, the problem is to provide low loss magnetic material with weak dispersion behavior at GHz frequencies. New miniaturization of the antennas would use the piezoelasticity and magnetoelasticity that has recently drawn great attention, in which the magnetoelectric (ME) effect is involved. The ME effect can be created by single-phase multiferroics or laminated composite materials, where the composite materials achieve a larger ME effect at room temperature. The ME laminated

composite was first introduced in 2001, since then, strong ME effects have been discovered in many laminated composites [4]–[6].

The ME coupling strength in these devices depends on the magnetostrictive and piezoelectric phases, as well as the interface bonding layers. These structures excite acoustic waves inside the device by creating magnetoelectric coupling between magnetostrictive and piezoelectric parts. Therefore, the structure works with acoustic wave resonance instead of electromagnetic resonance. Since the acoustic wavelength is much shorter than the electromagnetic wavelength at the same operating frequency, the ME structure is expected to show a resonance at much lower frequencies than the metallic antennas in the form of a loop or a dipole. Another positive point about the ME antenna is that, unlike the conventional antennas, it does not show the platform effect since the image current acts as in-phase radiation because of the magnetic nature of the created current on the structure [7].

Many papers have studied the performance of ME antennas numerically, analytically, and experimentally [8], [9]. In [8], ME antennas based on nano-plate resonator (NPR) and thin-film bulk acoustic wave resonator (FBAR) structures have been introduced. The measurement results show a promising future for this type of antenna in miniaturizing. The potential application of ME antenna is proposed in [10], in which an array of ME antennas has been introduced for biomedical use. The simulation of the ME antenna has been implemented in COMSOL Multiphysics® in [11] for the neafield communications in which the CST Studio® is used to calculate the nearfield coupling. Recently, theoretical analyses on fundamental performances of ME antenna with a focus on wireless power transfer have been presented [12], [13]. The equivalent circuit models and two-port network theory have been utilized to predict the performance of the ME structures [13], where an explicit closed-form equation has been derived and validated by different sets of rigorous experiments. In [12], the compact closed form of the optimal load impedance and its corresponding maximum output power is developed for wireless power transfer purposes. In [14], the radiation Q factor of the antenna has been calculated, and the comparison has been made by a 1-D multiscale FDTD code. However, the effect of nearfield around the antenna structure, as well as the effect of the feeding network, has not been included in the calculation of the Q factor. In [15], an unconditionally stable FDTD algorithm is proposed; the model accounts for ferromagnetic resonance since it solves the Landau–Lifshitz–Gilbert equation for the spin precessional motion. However, the model does not explain the effect of prestress created by the magnetic DC bias field. In [16] a dynamic finite element model has been introduced to solve the coupling between elastic mechanics and linear electromagnetism to calculate the radiation from an ME antenna. However, the nonlinear properties of magnetostrictive material have not been taken into account. To simulate magnetostrictive materials, different nonlinear models have been introduced in the literature, such as the standard square model [17], a model based on the density of domain switching, and the hyperbolic tangent model [18].

In this paper, the nonlinear model proposed in [9] is used for magnetostrictive material since the experimental data shows that the proposed model can accurately describe the nonlinear behavior and saturation trend of magnetostrictive material. In a real scenario, the nonlinear model might not be isotropic since the material sputtering changes its properties in different crystal directions. However, for the sake of simplicity, we have considered the nonlinear isotropic model for the magnetostrictive material FeGaB which is available in the literature [8]. The simulation has been validated by experimental data provided in [19]. We examine the performance of the structure through a multiphysics finite element method which predicts the nonlinear behavior of the magnetostrictive material. We have used different physics, i.e., structural mechanics, electrostatics, and magnetic field as well as two different couplings among solid mechanics and electrostatics and magnetic field. The coupling between solid mechanics and electrostatics simulates piezo-elasticity in the piezoelectric material, and the coupling between solid mechanics and magnetic field simulates the magnetoelasticity in magnetostrictive material. Since the ME structure behaves like a magnetic dipole, we compare its nearfield and farfield performances with a micro-loop of the same size. To this end, we use COMSOL Multiphysics® and CST Studio® for nearfield and farfield simulations, respectively. As a use case, we have simulated the ME antenna in the biomedical medium since it offers miniaturization without affecting the antenna impedance characteristics, easy integration with the metal ground plane, and low loss in the nearfield due to the magnetic near field nature of the antenna. These features make the antenna an appropriate choice in WBAN applications such as wireless communication and wireless powering of leadless cardiac pacemaker capsules [20], deep brain stimulators [21], and under skin RFID sensor implants [22].

The paper is organized as follows. Section II introduces the finite element formulation implemented in COMSOL Multiphysics®. Section III shows the ME antenna structure which contains AlN and FeGaB as the piezoelectric and the magnetostrictive materials, respectively. Section IV explains how the DC and AC simulations in COMSOL have been implemented together with the different physics. In section V the simulation has been validated with the measurement results from [19]. Finally, section VI discusses the different results from simulations along with the comparison between ME and micro-loop antennas.

II. FINITE ELEMENT FORMULATION

To simulate the magnetic field variation around the ME antenna, we have used two-step simulations. First, we use the nonlinear model to calculate the prestress created by DC magnetic field, which is called the bias point. Then, the dynamic variation of the magnetic field, which is a small oscillation about the bias point, has been calculated by small-signal magnetization. To formulate the structure, different

physics has been considered as follows:

A. SOLID MECHANICS

The equilibrium equation in solid mechanics is written using a spatial formulation in terms of the Cauchy stress tensor S

$$\nabla \cdot S + \mathbf{F}_V = -\rho\omega^2\mathbf{u}, \tag{1}$$

where $\mathbf{F}_V$ is the body force per unit volume, ρ is the mass density, ω is the applied frequency, and $\mathbf{u}$ is the displacement. In the static case, the right side of (1) will be zero. In addition, the infinitesimal strain tensor (ϵ) is defined as

$$\epsilon = \frac{1}{2}(\nabla\mathbf{u} + (\nabla\mathbf{u})^T). \tag{2}$$

Two different responsive materials, namely magnetostrictive and piezoelectric, are used in the structure. Their behavior is formulated in subsections (II-B) and (II-D), respectively.

B. MAGNETOSTRICTIVE MATERIAL

To simulate the nonlinear and saturation behavior of the magnetostrictive material, we have used the model introduced in [9], which is available in COMSOL Multiphysics®. The magnetostrictive constitutive relations can be expressed in the following general form [9]

$$\begin{cases} \varepsilon_{ij} = \varepsilon_{ij}^0(\sigma_{kl}) + \varepsilon_{ij}^1(M_k, \sigma_{mn}), \\ \boldsymbol{H}_k = \boldsymbol{H}_k^0(M_l) + \boldsymbol{H}_k^1(M_l, \sigma_{mn}), \end{cases} \tag{3}$$

where $\mathbf{H}$ is the magnetic field strength and $\varepsilon_{ij}^0(\sigma_{kl})$, is the elastic strain produced by prestress. After applying symmetry for isotropic magnetostrictive materials, the nonlinear strain is modeled as follows

$$\varepsilon_{me} = \frac{\lambda_s}{M_s^2}\left(\frac{3}{2}M_iM_j - \frac{1}{2}M_kM_k\delta_{ij}\right), \tag{4}$$

where, λ_s, M_s and δ_{ij} are saturation magnetostriction, saturation magnetization, and the Kronecker delta, respectively. Using (4), we can derive a linear response around a given bias point characterized by the vector $\mathbf{M}_0$ = [0,M_0,0] along with a small-signal magnetization characterized by vector m = [m_1,m_2,m_3]. The bias magnetic field is defined in the y direction, As a result, (4) can be simplified as

$$\varepsilon_{me} = \frac{\lambda_s M_0}{M_s^2}\left[-m_2, 2m_2, -m_2, 3m_3, 0, 3m_1\right]. \tag{5}$$

The stress in the magnetostrictive material is described as

$$S = c_H\left[\varepsilon - \varepsilon_{me}(\boldsymbol{M})\right], \tag{6}$$

where c_H is the stiffness matrix. Nonlinear magnetization in the magnetostrictive material is found from the following nonlinear implicit relation,

$$\boldsymbol{M} = M_s(coth(x) - \frac{1}{x})\frac{\boldsymbol{H}_{eff}}{|\boldsymbol{H}_{eff}|}; \qquad x = \frac{3\chi_m|\boldsymbol{H}_{eff}|}{M_s}, \tag{7}$$

where, for the nonlinear scalar function, the Langevin function $[\coth(x) - 1/x]$ has been used and χ_m is the magnetic susceptibility in the initial linear region. For cubic crystals, the effective magnetic field intensity in the material is given by

$$\boldsymbol{H}_{eff} = \boldsymbol{H} + \frac{3}{2}\frac{\lambda_s}{M_s^2}dev(c_H\varepsilon)\boldsymbol{M}, \tag{8}$$

where $\mathbf{H}$ is the applied magnetic field, the second term in (8) is the mechanical stress contribution to the effective magnetic field intensity, and dev is the deviatoric operator.

Finally, we use Maxwell's equations to account for the change in the magnetic field as a result of the magnetization change in the magnetostrictive material.

C. MAGNETIC VECTOR POTENTIAL

Because of the divergence-free nature of the magnetic flux density, one can define magnetic vector potential $\mathbf{A}$ to calculate the field components. This implies that it is possible to rewrite Maxwell's equations in the following forms

$$\begin{cases} \boldsymbol{B} = \nabla\times\boldsymbol{A}, \\ \nabla\times\boldsymbol{H} = \boldsymbol{J}_e + \sigma\boldsymbol{E} + j\omega\boldsymbol{D}, \\ \boldsymbol{E} = -j\omega\boldsymbol{A}, \\ \boldsymbol{B} = \mu_0(\boldsymbol{H} + \boldsymbol{M}), \end{cases} \tag{9}$$

where $\mathbf{B}$ is the magnetic flux density, $\mathbf{H}$ is the magnetic field strength, $\mathbf{J}_e$ is the external current density, σ is the electrical conductivity and $\mathbf{D}$ is the electric displacement field. Here, with the gauge transformation $\widetilde{\boldsymbol{A}} = \boldsymbol{A} - \frac{j}{\omega}\nabla\varphi$, $\widetilde{\varphi} = 0$, (9) can be written as follows.

$$\left(j\omega\sigma - \omega^2\varepsilon\right)\boldsymbol{A} + \nabla\times\left(\mu_0^{-1}\nabla\times\boldsymbol{A} - \boldsymbol{M}\right) = 0. \tag{10}$$

D. PIEZOELECTRIC MATERIAL

The constitutive relation in the piezoelectric material can determine the coupling between the stress and the electric field [23] as follows,

$$\begin{cases} \varepsilon = s_E S - d^T\boldsymbol{E} \\ \boldsymbol{D} = dS + \varepsilon_0\varepsilon_T\boldsymbol{E}, \end{cases} \tag{11}$$

where the material parameters s_E, d, and ε_T, correspond to the material compliance, the coupling properties, and the permittivity. To simulate the physics involving the piezoelectric material Gauss law equation should be solved as well

$$\nabla.\boldsymbol{D} = \rho_V, \tag{12}$$

where $\mathbf{D}$ is the electric displacement field and ρ_V is the free electric charge density. The electric field is computed from the electric potential V as

$$\mathbf{E} = -\nabla\boldsymbol{V}. \tag{13}$$

In the transmitting mode, the applied AC voltage to the piezoelectric terminal will create the electric field variation inside the piezoelectric material, which in turn creates the strain in the piezoelectric material.

E. MULTIPHYSICS COUPLING

Figure. 1, shows the transmitting mode of the ME antenna heterostructure, when the voltage is applied to the piezoelectric terminals, a strain wave in the piezoelectric material is created that is directly transferred to the piezomagnetic (magnetostrictive) material, this strain wave will induce a dynamic change of magnetization inside the piezomagnetic which in turn will create radiation. Conversely, in the receiving mode, the dynamic magnetic field (RF wave) creates a strain wave in piezomagnetic material, which is transferred to the piezoelectric material, this strain wave inside the piezoelectric material will then create voltage in the piezoelectric terminals.

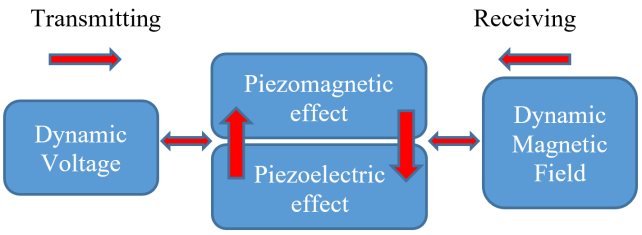

FIGURE 1: Coupling mechanism in the ME antenna. In the transmitting mode the dynamic voltage creates a dynamic magnetic field through piezoelectric and piezomagnetic effects and in the receiving mode the process is reversed.

To calculate the multi-physic effect, first, the DC magnetic bias field is applied to the magnetostrictive material to create a prestress inside the structure. To this end, a uniform background magnetic flux density has been defined. The prestress accounts for the nonlinear part of the elastic strain, which is responsible for the change of the maximum magnetostrictive strain created in the structure [9]. To calculate the prestress, we solve (1), (4), (6)-(8), (10) in which ω equals zero in (1), (10). To calculate the dynamic magnetic field intensity created by the AC voltage in the piezoelectric part of the ME antenna, two different multiphysics couplings should be solved. First, piezoelectric physics which combines solid mechanics and electrostatics in which, (1), (2), (11)-(13) will be solved. Here we assume that the electrostatic formula is valid in the time-harmonic study since the electromagnetic wavelength and skin depth are very large compared to the size of the structure. Second, magnetostrictive physics that couples solid mechanics and magnetic field, in which (1), (2), (5)-(8), (10) are involved.

III. STRUCTURE

The resonant bodies of the magnetoelectric antenna resonators are AlN and FeGaB heterostructures fully suspended in air, where AlN and FeGaB serve as the piezoelectric and magnetostrictive element of the ME heterostructure, respectively (see Fig. 2). Appendix I provides the material properties of FeGaB and AlN. The antenna size and different loss mechanisms are given in Table 1.

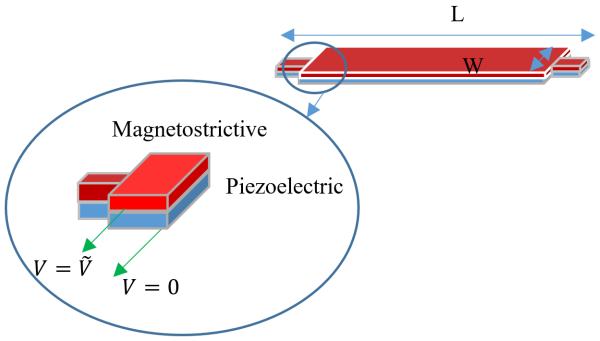

FIGURE 2: ME antenna consisting of the magnetostrictive and piezoelectric. The voltage is applied to the piezoelectric terminals.

TABLE 1: THE CHARACTERISTICS OF THE STRUCTURE

Property	Value
Magnetostrictive thickness	$0.5\ [\mu m]$
Piezoelectric thickness	$0.5\ [\mu m]$
Length of the structure (L)	$250\ [\mu m]$
Width of the structure (W)	$50\ [\mu m]$
Magnetic DC bias	$2 - 50\ [mT]$
Mechanical damping loss η_s in the Magnetostrictive material	$1e-4$
Mechanical damping loss η_s in the piezoelectric Material	$1e-4$
Dielectric loss in the piezoelectric material $\tan\delta$	$1e-3$

IV. COMSOL SIMULATION

In COMSOL Multiphysics®, we have utilized the AC/DC module together with Structural Mechanics module to simulate the ME antenna. In AC/DC module we have used Magnetic Field physics and Electrostatics physics and in the Structural Mechanics module, we have activated Solid Mechanics physics. As shown in Fig. 3, two different simulations i.e. DC and AC simulations are carried out with the Stationary solver and Frequency-Domain Perturbation solver, respectively. The simulation result from the DC simulation is used as the operating point for the AC simulation. Despite using the nonlinear model for the magnetostrictive material and sophisticated coupling between different physics, the simulation in COMSOL converges after a few iterations. The simulations are categorized as follows,

A. DC SIMULATION

The DC simulation is carried out by the Stationary solver, in which the magnetic physics and solid mechanic physics are coupled in the multiphysics branch in COMSOL. The magnetostriction effect accounts for the magnetostrictive effect i.e. Joule effect and the inverse magnetostrictive effect i.e. Villari effect as shown in Fig. 3. In this case, the dependent variables are magnetic vector potential $\mathbf{A}$, magnetization $\mathbf{M}$ and displacement $\mathbf{u}$. The result of the stationary solver defines the bias point for the magnetostrictive material. The solver type is PARDISO (parallel sparse direct solver) with the direct method to solve the fully coupled equations. For the solid parts, we have considered hexahedral mesh which

includes 376 mesh elements, and for the air surrounding it, the tetrahedral mesh has been applied which has 49927 mesh elements. In addition, for the Infinite Element Domain surrounding the air, we have used five layers of swept mesh with 8140 mesh elements. To model the unbounded domain for air surrounding the structure we have activated the Infinite Element Domain node. In addition, in order to consider the magnetic DC bias we have activated the uniform background magnetic flux density in Magnetic Field physics. The simulation is performed on a desktop computer with 128 GB memory and an Intel Core i7-7820X CPU running at 3.60 GHz which on average takes about 134s to be completed.

B. AC SIMUALTION

The AC simulation uses the Frequency-Domain Perturbation solver, in which, as shown in Fig. 3, the Magnetic physics and Solid Mechanic physics are coupled to get the magnetostrictive and inverse magnetostrictive effects together with the coupling between Solid Mechanics and Electrostatics physics which gives the piezoelectric and inverse piezoelectric effects. In this case, the dependent variables are magnetic vector potential **A**, magnetization **M**, displacement **u** and electric potential V. Here, the result of the DC simulation is used as the working point to apply a small signal study, in which, 1 mV AC signal (perturbation) is applied to the piezoelectric terminals as a voltage source. The solver type and the mesh settings are the same as DC simulation and the Infinite Element Domain node is activated as well to model an infinite medium around the structure. The simulation time and memory for a single frequency are 450 s and 35 GB, respectively.

V. VALIDATION OF SIMULATION

To validate the simulation of the ME antenna, first we use an example of the array of three ME antennas with the same size and material properties as developed in [19]. The setup is shown in Fig. 5, the array consists of three ME antennas with the size of 250 μm × 50 μm which are 12 μm apart. The power transfer efficiency (PTE) of the ME antenna array has been measured at different distances from the transmitter (T_x) coil. The structure shows three different modes of operation: along width, length, and thickness. Here, we use the thickness modes of the ME resonators since it shows higher efficiency than the width and length modes [19]. The resonance frequency for thickness mode is as follows [19]

$$f_{\text{thickness mode}} = \frac{1}{2t}\sqrt{\frac{E_{eq}}{\rho_{eq}}}, \tag{14}$$

where t is the thickness of the piezoelectric, and E_{eq} and ρ_{eq} are the equivalent Young's modulus and equivalent density of the structure, respectively.

The thickness mode in COMSOL simulation resonates in 2.471 GHz, Fig. 4 shows the measured and simulated return loss S_{11}, the measured plot is taken from [19]. The simulated S_{11} resonates in a lower frequency i.e. 30 MHz

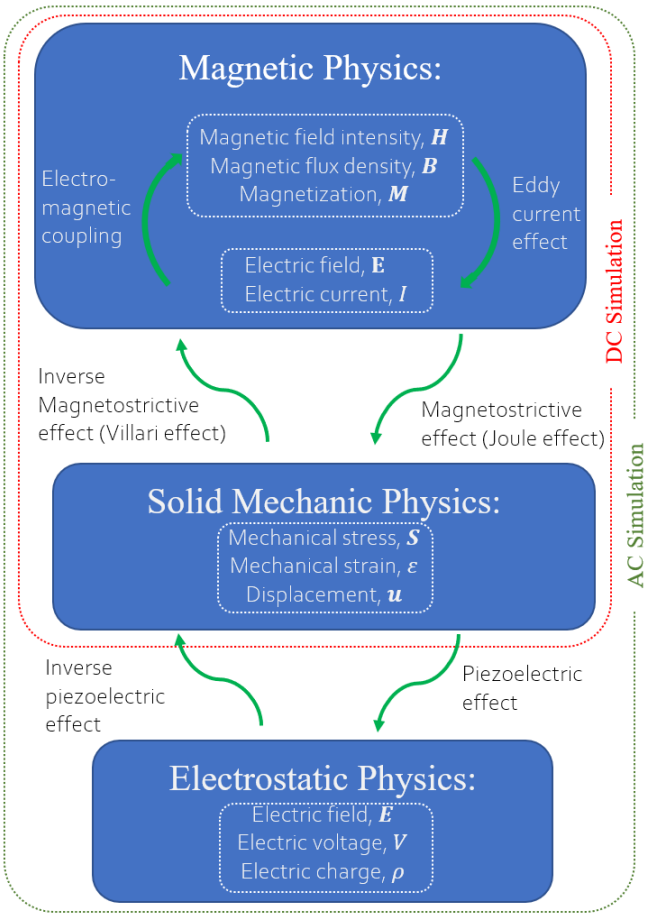

FIGURE 3: The Coupling diagram: the coupling in the Magnetic physics i.e. eddy current effect and electromagnetic coupling, the coupling between Magnetic and Solid Mechanic physics i.e. Joule and Villari effects, the coupling between Solid Mechanics and Electrostatics physics i.e. piezoelectric and inverse piezoelectric effects.

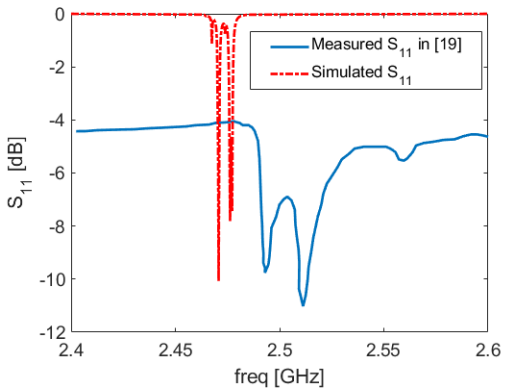

FIGURE 4: The measured and simulated S_{11}. Measured plot from [19] and simulated plot in COMSOL.

is lower than the measured resonance and it shows lower bandwidth. One possible explanation for the frequency shift

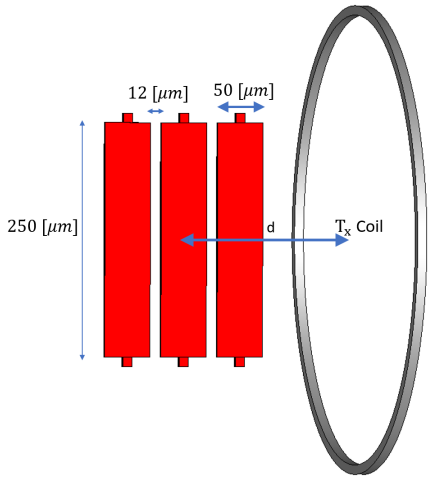

FIGURE 5: Setup used in [19]. An array of ME antennas with the size of 250 µm × 50 µm which are 12 µm apart from each other (for illustration purposes, the ME size is magnified). The power transfer efficiency (PTE) has been calculated between the T_x coil and the array of ME antennas at different distances between them.

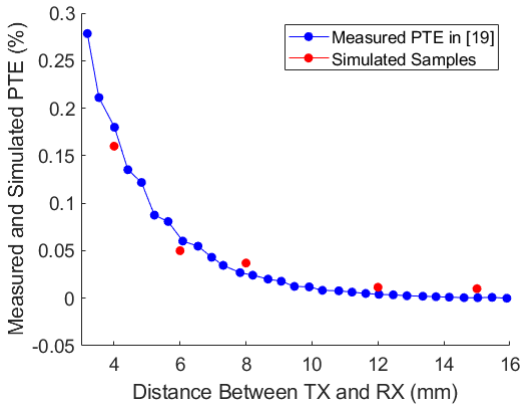

FIGURE 6: The measured PTE from [19]. The red dots show the simulated samples in COMSOL.

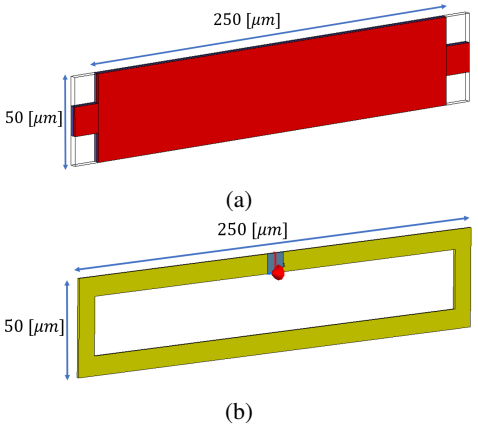

FIGURE 7: The transmitter antennas with the same size 250 µm × 50 µm, (a) ME antenna, (b) micro-loop with copper $\sigma = 5.96 \times 10^7$.

could be due to tolerances of the fabrication process. The presence of the lossy materials in the measurement increases the bandwidth which may explain the high bandwidth of the measurement result compared to the simulated one. To calculate the coupling, a 37 Oe DC bias field is provided in the ME antennas through the background magnetic DC bias in order to create a prestress inside the magnetostrictive material FeGaB. In COMSOL we have simulated the coupling for a few samples for different distances between the T_x coil and ME antenna. As shown in Fig. 6 the simulated results are in good agreement with the measurements. After validation, we use a single element ME antenna to simulate the antenna gain and radiation pattern as well as its the antenna nearfield performance. To make a comparison with electrical antennas, we use a micro-loop as an equivalent magnetic antenna and compare the ME and the loop performances.

VI. ME ANTENNA VERSUS MICRO-LOOP

The performance of the ME antenna is studied in the following subsections in which we present the input impedance, equivalent magnetic current, farfield, nearfield, as well as a use case in biomedical implans. The nearfield simulations are performed in COMSOL Multiphysics® and for the farfield simulation such as gain and radiation pattern we use CST Studio®. We show that the ME antenna performs are much better than a micro-loop of an equivalent size (see Fig. 7), either in farfield radiation in free space, antenna nearfield for wireless communication and wireless powering as well as in the biomedical implant use case.

A. INPUT IMPEDANCE

To calculate the input impedance, we have applied an AC voltage to the piezoelectric material in COMSOL. Electrostatic simulations are used that is valid in the AC simulation as well since the piezoelectric thickness compared to the wavelength is very small. In the ME antenna, different loss mechanisms such as mechanical damping in piezoelectric and magnetostrictive material as well as the electrical loss affects the input impedance, these losses are given in Table 1. The real and imaginary parts of the input impedance of the ME antenna are plotted in Fig. 8. The micro-loop, with the size of λ/500, shows a very small resistivity which makes it difficult to match to 50 Ω impedance. In Fig 9. the return loss of the ME antenna with magnetic DC bias 20 mT as well as the micro-loop are shown, the reference impedance for calculating the return loss is 50 Ω. As shown, the ME antenna has much lower return loss than the micro-loop, the antenna resonates at 2.4705 GHz and 2.477 GHz, and the input impedances in these frequencies are 28.6+j47 Ω and 51.6+j46 Ω, respectively.

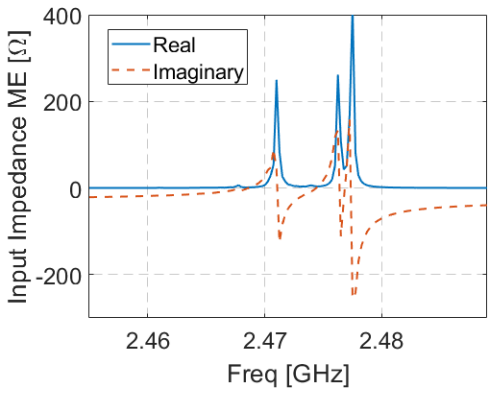

(a)

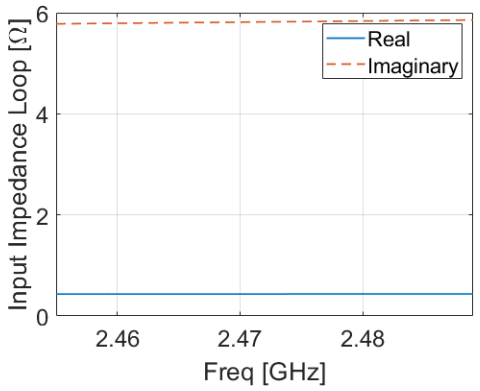

(b)

FIGURE 8: Input impedance, (a) ME antenna with magnetic DC bias 20 mT, (b) micro-loop with copper σ = 5.96 $\times 10^7$. The antennas are shown in Fig. 7.

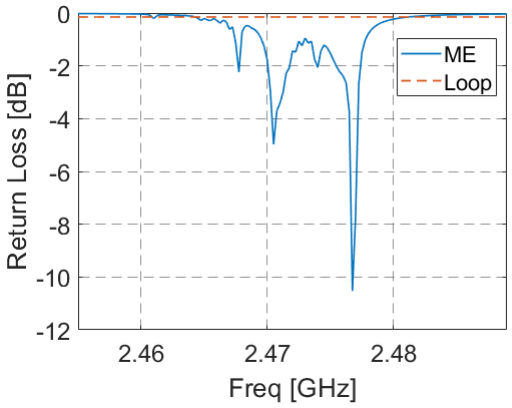

FIGURE 9: Return loss of the ME antenna with magnetic DC bias 20 mT and micro-loop with copper σ = 5.96 $\times 10^7$. The antennas are shown in Fig. 7.

B. EQUIVALENT MAGNETIC CURRENT

With the stress and strain created in the magnetostrictive material, the ME antenna produces an equivalent magnetic current. This current creates the variation of the magnetic field intensity around the ME antenna which is shown in Fig. 10. a. To simulate the AC magnetic field intensity around the structure, first, we apply the magnetic DC bias to the ME antenna to calculate the bias point in which the nonlinear (4) is solved together with (1), (6)-(8), (10) where ω is equal to zero in (1),(10). After calculating the bias point, we use the linearized equation (5) along with (1)-(2), (6)-(8), (10)-(13) to calculate the AC change. Then, we apply AC voltage to the piezoelectric terminal, the AC voltage creates AC vibration in the piezoelectric material. Subsequently, this vibration creates AC magnetostrictive strain which in turn results AC magnetic field intensity around the antenna. In Fig. 10. b, the equivalent magnetic current $\mathbf{M}=-\nabla \times \boldsymbol{E}$ has been plotted, as shown, the current superposition is in the same direction as the magnetic DC bias since the dynamic variation of the magnetic current acts as the perturbation to the DC magnetic bias. As we know from the image theory, Fig. 10. c, the equivalent magnetic current, and its image are in the same direction when the magnetic current is parallel to the perfect electric conductor (PEC) ground plane. Therefore, in this case, the equivalent magnetic current will be doubled. Therefore, as discussed previously, the ME antenna does not have the platform effect.

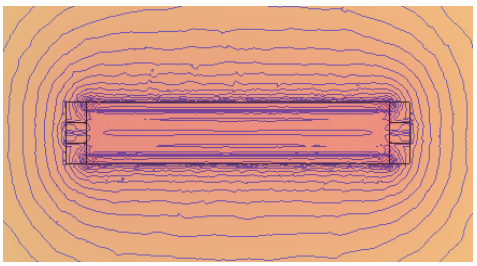

(a)

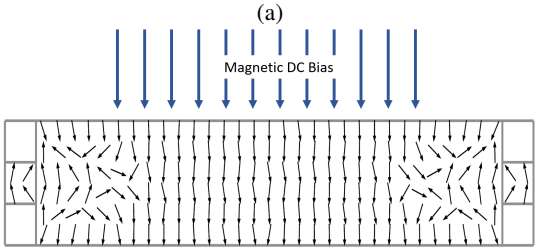

(b)

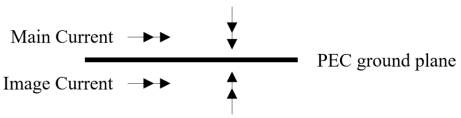

(c)

FIGURE 10: Field display of the ME antenna, (a) Magnetic field lines created around the ME antenna, (b) Equivalent magnetic current created on the surface: arrows show the field direction, (c) Image of magnetic current above the PEC ground plane, the horizontal and vertical image currents are in phase and out of phase, respectively.

C. ANTENNA FARFIELD

To study the radiation pattern of the ME antenna we need to extract the nearfield of the structure. We calculate the nearfield around the ME antenna using FEM method in COMSOL Multiphysics® then we extract and use the calculated nearfield as a source of Maxwell's Equations in CST Studio® to calculate the gain of the ME antenna. According to the surface equivalence theorem, if the materials and the surrounding environment are linear, a structure generating electromagnetic fields can be replaced by a set of electric and magnetic surface current densities existing on a surface surrounding the structure [24]. Even though the materials being used in the antenna's structure are not linear, the structure can be assumed linear due to the linearization of the nonlinear model of the magnetostrictive material. After linearization, small-signal perturbation as a voltage has been applied to the piezoelectric. If we consider the ME and micro-loop antennas as Fig. 7, in which the bias direction for the ME antenna is assumed to have the same direction as the equivalent magnetic dipole moment of the micro-loop, they both will have the same radiation pattern because both antennas behave as the magnetic dipole. The farfield simulation in the CST shows that both antennas are omnidirectional in the azimuth direction, the gain of the antennas with respect to the elevation angle is shown in Fig. 11. The gain for ME antenna biased with 20 mT and micro-loop antenna are -61.25 and -70.3 dB, respectively. However, in practice, we will have the realized gain which is -63.5 and -84 dB for the ME and micro-loop antennas, respectively. The realized gain accounts for the antenna impedance matching as well. Therefore, the ME antenna shows almost 20 dB better performance than the micro-loop with the same size because the micro-loop, with the size of λ/500, shows a great mismatch to 50 Ω load, whereas the ME antenna shows a better matching to 50 Ω load (see Fig. 9).

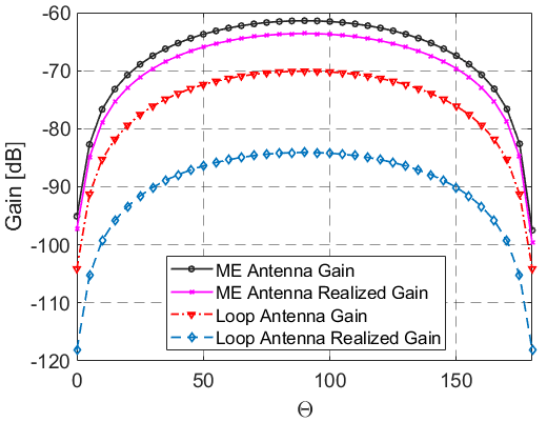

FIGURE 11: Antenna gain for the ME and micro-loop antennas with respect to elevation angle, ME antenna gain: -61.25 dB, ME antenna realized gain: -63.5 dB, micro-loop gain: -70.3 dB, micro-loop realized gain: -84 dB.

D. NEARFIELD COMMUNICATION

To calculate the return loss and the coupling between the ME antenna and receiver (R_x) loop we use a similar setup like the one shown in Fig. 5. However, here, we use a single element ME antenna and different biases are applied to the ME antenna as a background field. The distance between the ME antenna and R_x loop is fixed at 5 mm. In addition, the mismatch effect of the R_x antenna has been de-embedded from the coupling efficiency by using the following formula,

$$\eta = \frac{S_{21}^2}{1 - S_{22}^2} \tag{15}$$

where S_{22} is the reflection from the R_x loop and S_{21} is the transmission coefficients between the ME antenna and R_x loop, respectively. The same setup is also used to calculate the coupling between the micro-loop and the same R_x loop. The return loss is shown in Fig. 12 with reference impedance 50 Ω, as shown, the ME antenna shows two resonances that are only about 5 MHz apart from each other. However, we are interested in the first resonance which occurs in the lower frequency since the coupling shows better performance for the first one. The magnitude and location of the resonances depend on the magnetic DC bias applied to the ME antenna because the bias changes the prestress created inside the magnetostrictive material which in turn changes the resonance frequency. Unlike the ME antenna, the return loss for the micro-loop in Fig. 12 shows that the high percentage of the power reflects from the input port and it is difficult to make a practical matching-network for the micro-loop.

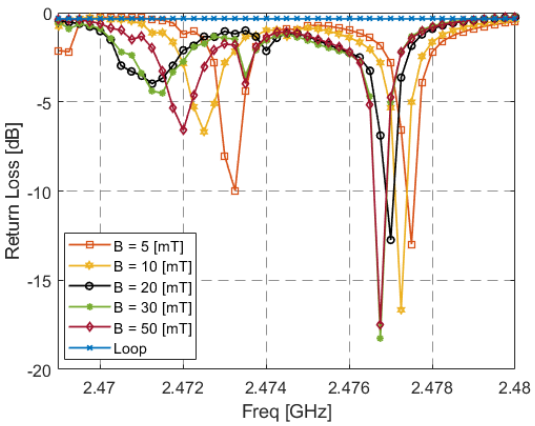

FIGURE 12: Return loss of the ME antenna for different DC magnetic biases together with micro-loop.

In Fig. 13 the coupling between the ME antenna and R_x loop for different DC magnetic biases has been plotted together with the coupling between micro-loop and the same R_x loop. As shown, with the DC magnetic bias of 20 mT, the coupling with the ME antenna is 13 dB better than the micro-loop with the same size. The coupling first increases with higher magnetic bias but after saturation of the magnetostrictive material the coupling starts to decrease. The

best coupling which is achieved here is with 20 mT, and the performance of the ME antenna with bias as small as 5 mT is better than the micro-loop.

As discussed in section VI.B the bias direction defines the direction of the equivalent magnetic dipole of the ME antenna, the DC bias must be in line with the AC magnetic field of the R_x loop to provide maximum efficiency. If they are perpendicular the efficiency drops significantly. To show this, we have simulated four different cases shown in Fig. 14 (a) together with their coupling efficiency curve as shown in Fig. 14 (b). The aligned bias with the AC magnetic field of the R_x loop i.e. case I and case II, show maximum efficiency with slightly different values, while the perpendicular biases have minimum coupling i.e. case III and case IV. In this paper, we have studied case I since it has been used in [19] and we validated the simulation results with the measurements in this reference.

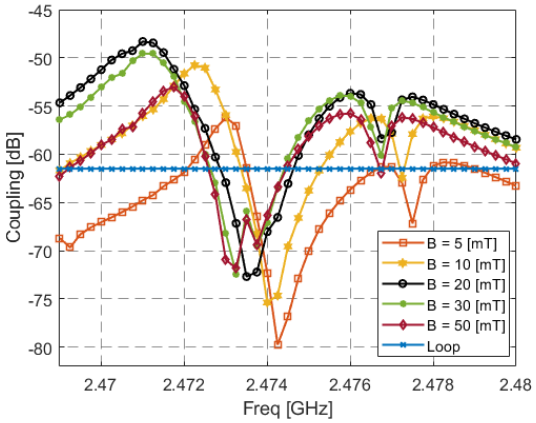

FIGURE 13: Coupling between the ME antenna and R_x loop for different DC magnetic biases along with the coupling between micro-loop and the same R_x loop.

E. BIOMEDICAL APPLICATIONS

In order to study the performance of the ME antenna in the biomedical medium, we consider the coupling-setup in the tissue environment as Fig. 15. The ME antenna and micro-loop are located in the hollow cube with a 0.5 mm edge size created in the muscle. The muscle size is 10 mm × 10 mm × 25 mm and the R_x coil with a 4 mm diameter is located as an on-body receiver with a 0.25 mm distance from the muscle surface. The surrounding muscle has $\sigma = 1.753$ and $\varepsilon = 52.7 + j0.24$ at 2.47 GHz [25]. We consider two scenarios, first, the coupling between the ME antenna and the R_x loop, and second, the coupling between micro-loop and the same R_x loop. The ME and micro-loop antennas are shown in Fig. 7, the ME antenna has 20 mT magnetic DC bias and micro-loop is made of copper with $\sigma = 5.96 \times 10^7$.

In Fig. 16 the coupling in the tissue environment versus the distance between the T_x and the R_x is shown. The coupling for the first scenario is at least 10 dB better than the second scenario, for both the air and muscle embedded antennas.

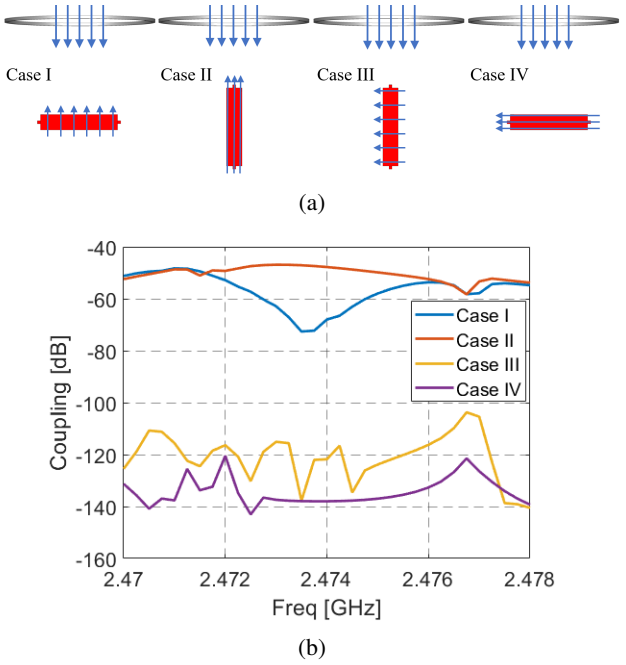

FIGURE 14: Rotation of the ME antenna with different orientation of DC magnetic bias with respect to AC magnetic field of the R_x loop and their coupling plot. The DC bias is 20 mT and for illustration purposes, the ME size is magnified. (a) four different cases of the ME antenna bias and orientation; case I: bias along width and parallel with AC field, case II: bias along length and parallel with AC field, case III: bias along width and perpendicular to AC field, case IV: bias along length and perpendicular to AC field. (b) the coupling result for case I- IV.

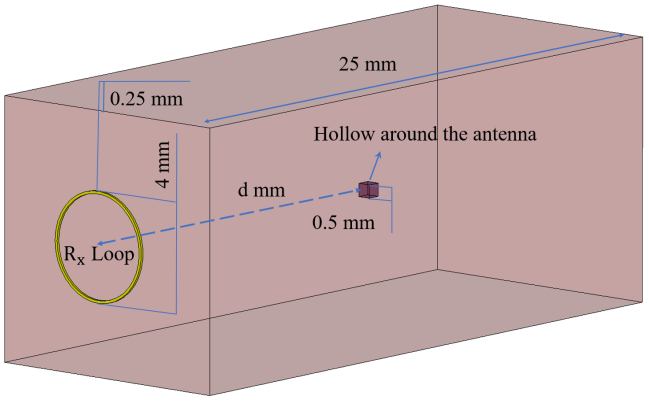

FIGURE 15: The coupling-setup in the tissue environment. The ME antenna is located in the hollow cube with a 0.5 mm edge size created in the muscle and the R_x loop with a 4 mm diameter is located as an on-body receiver with a 0.25 mm distance from the muscle surface.

As shown in Fig. 16 the coupling with using ME or the micro-loop in the muscle, at a close distance (<7mm) to the reference loop is reduced compared to the air, due to the antenna nearfield loading by the lossy muscle tissues. However,

beyond 7mm distance, the coupling in the muscle scenario is higher than the air because the embedded antenna has a larger physical size compared to the antenna in free space [26]. In addition, in the simulation, the return loss for the ME antenna when surrounded by the muscle is almost the same as when surrounded by air which accounts for the fact that in the ME antenna contribution of the mechanical loss in the input impedance is the dominating part as the structure resonates in its mechanical thickness mode. Therefore, conductivity and dielectric loss from muscle do not create a significant shift in the resonance frequency. In biomedical implants in which the electrical conductivity of the medium around the antenna varies due to the surrounded tissues, the ME antenna offers better impedance matching since the mechanical mode does not change by the electrical conductivity or dielectric loss of the medium. Therefore, the ME antenna is a promising alternative for biomedical implants. However, it has some limitations such as design and simulation complexity and high manufacturing costs since the technology is still immature and mainly used in the research community.

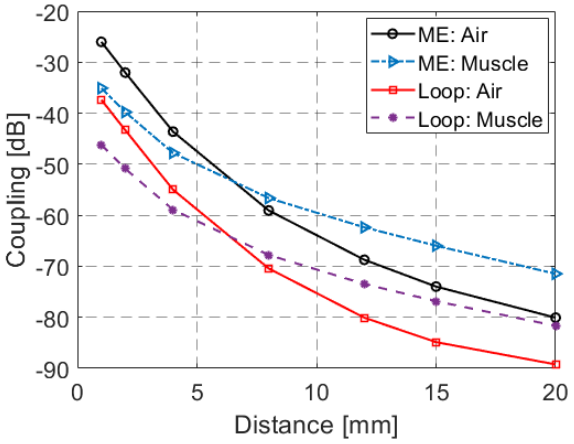

FIGURE 16: Efficiency of the antennas versus distance. ME antenna has 20 mT DC bias, micro-loop made of copper σ = 5.96 ×10^7. Muscle properties: $\sigma = 1.753$ and ε = 52.7 + j0.24

VII. CONCLUSION

Magnetoelectric (ME) material is a new technology with significant potential in antenna miniaturization. ME antenna modeling is the first step toward designing complex antenna geometries. In this paper, we have focused on the COMSOL Multiphysics® modeling and simulations of the antenna. The nonlinear isotropic model is considered for magnetostrictive material to simulate the effect of DC magnetic bias which has been simulated through the stationary solver in COMSOL, then the perturbation solver has been applied to account for the dynamic oscillation of the structure in the resonance frequency. It is shown that the ME antenna behaves like a magnetic dipole similar to a micro-loop with the same radiation pattern but with approximately 20 dB higher realized gain. The generated magnetic dipole moment is in parallel to the magnetic DC bias of the structure. Unlike the micro-loop, with the size of λ/500, which acts like a short-circuit at 2.471 GHz, the input impedance of the ME antenna depends on the acoustic resonance in the structure and it offers better matching to a 50 Ω load impedance. Moreover, the coupling performance of the ME antenna is evaluated and compared to the micro-loop which performs 10 to 13 dB better than the micro-loop in both air and muscle tissue at different distances from an R_x loop. As a result, the ME antenna shows a promising future in both farfield and nearfield communication devices due to having a low profile, low return loss, low structural loss, high gain and coupling performance. Therefore, the ME antenna can be a good choice for different biomedical applications where the antenna efficiency and miniaturization are the main goals.

APPENDIX I

The material properties for magnetostrictive and piezoelectric materials are as follows,

A. MAGNETOSTRICTIVE

FeGaB has been used as a magnetostrictive material, to use the nonlinear isotropic model of FeGaB the following parameters have been considered in the simulation, [8],

Density: 7860 kg/m³
Young's modulus: 55 GPa
Poisson's ratio: 0.27
Electrical conductivity: 2e5 S/m
Relative permittivity: 1
Saturation magnetization: 1114084 A/m
Saturation magnetostriction: 70 ppm

B. PIEZOELECTRIC

To model the piezoelectric material parameters such as s_E, d, and ε_T, which correspond to the material compliance, the coupling properties, and the permittivity are needed. These quantities are tensors of rank 4, 3, and 2, respectively. The AlN material properties are as follows,

$$S_E = \begin{bmatrix} 2.9 & -0.93 & -0.5 & 0 & 0 & 0 \\ -0.93 & 2.9 & -0.5 & 0 & 0 & 0 \\ -0.5 & -0.5 & 2.9 & 0 & 0 & 0 \\ 0 & 0 & 0 & 8 & 0 & 0 \\ 0 & 0 & 0 & 0 & 8 & 0 \\ 0 & 0 & 0 & 0 & 0 & 7.7 \end{bmatrix} \times 10^{-12} \frac{m^2}{N}$$

$$d = \begin{bmatrix} 0 & 0 & 0 & 0 & -3.8 & 0 \\ 0 & 0 & 0 & -3.8 & 0 & 0 \\ -1.9 & -1.9 & 5 & 0 & 0 & 0 \end{bmatrix} \times 10^{-12} \frac{C}{N}$$

$$\varepsilon_T = \begin{bmatrix} 9 & 0 & 0 \\ 0 & 9 & 0 \\ 0 & 0 & 9 \end{bmatrix}$$

The contribution of losses is considered by replacing ε_T with $(1 - j\,tan\,\delta)\,\varepsilon_T$ and c_E with $(1 + j\eta_s)\,c_E$ in which $c_E = S_E^{-1}$. Loss values are given in TABLE I.

REFERENCES

[1] Carl Pfeiffer. Fundamental efficiency limits for small metallic antennas. IEEE Transactions on Antennas and Propagation, 65(4):1642–1650, 2017.

[2] RC Hansen and Mary Burke. Antennas with magneto-dielectrics. Microwave and optical technology letters, 26(2):75–78, 2000.

[3] Hossein Mosallaei and Kamal Sarabandi. Magneto-dielectrics in electromagnetics: Concept and applications. IEEE Transactions on antennas and propagation, 52(6):1558–1567, 2004.

[4] Yanmin Jia, Haosu Luo, Xiangyong Zhao, and Feifei Wang. Giant magnetoelectric response from a piezoelectric/magnetostrictive laminated composite combined with a piezoelectric transformer. Advanced materials, 20(24):4776–4779, 2008.

[5] Peter Finkel, Samuel E Lofland, and Ed Garrity. Magnetoelastic/piezoelectric laminated structures for tunable remote contactless magnetic sensing and energy harvesting. Applied Physics Letters, 94(7):072502, 2009.

[6] A Lasheras, J Gutiérrez, and JM Barandiarán. Size effects in the equivalent magnetic noise of layered fe64co17si7b12/pvdf/fe64co17si7b12 magnetoelectric sensors. Sensors and Actuators A: Physical, 263:488–492, 2017.

[7] Hwaider Lin, Mohsen Zaeimbashi, Neville Sun, Xianfeng Liang, Huaihao Chen, Cunzheng Dong, Alexei Matyushov, Xinjun Wang, Yingxue Guo, Yuan Gao, et al. Future antenna miniaturization mechanism: Magnetoelectric antennas. In 2018 IEEE/MTT-S International Microwave Symposium-IMS, pages 220–223. IEEE, 2018.

[8] Tianxiang Nan, Hwaider Lin, Yuan Gao, Alexei Matyushov, Guoliang Yu, Huaihao Chen, Neville Sun, Shengjun Wei, Zhiguang Wang, Menghui Li, et al. Acoustically actuated ultra-compact nems magnetoelectric antennas. Nature communications, 8(1):1–8, 2017.

[9] Xin'en Liu and Xiaojing Zheng. A nonlinear constitutive model for magnetostrictive materials. Acta Mechanica Sinica, 21(3):278–285, 2005.

[10] Mohsen Zaeimbashi, Hwaider Lin, Cunzheng Dong, Xianfeng Liang, Mehdi Nasrollahpour, Huaihao Chen, Neville Sun, Alexei Matyushov, Yifan He, Xinjun Wang, et al. Nanoneurorfid: A wireless implantable device based on magnetoelectric antennas. IEEE Journal of Electromagnetics, RF and Microwaves in Medicine and Biology, 3(3):206–215, 2019.

[11] F Rangriz, A Khaleghi, and I Balasingham. Wireless link for microscale biomedical implants using magnetoelectric antennas. In 2020 14th European Conference on Antennas and Propagation (EuCAP), pages 1–4. IEEE, 2020.

[12] Binh Duc Truong and Shad Roundy. Experimentally validated model and power optimization of a magnetoelectric wireless power transfer system in free-free configuration. Smart Materials and Structures, 29(8):085053, 2020.

[13] Binh Duc Truong. Fundamental issues in magnetoelectric transducers: Magnetic field sensing versus wireless power transfer systems. IEEE Sensors Journal, 20(10):5322–5328, 2020.

[14] Zhi Yao, Yuanxun Ethan Wang, Scott Keller, and Gregory P Carman. Bulk acoustic wave-mediated multiferroic antennas: Architecture and performance bound. IEEE Transactions on Antennas and Propagation, 63(8):3335–3344, 2015.

[15] Zhi Yao, Sidhant Tiwari, Ting Lu, Jesse Rivera, Kevin QT Luong, Robert N Candler, Gregory P Carman, and Yuanxun Ethan Wang. Modeling of multiple dynamics in the radiation of bulk acoustic wave antennas. IEEE Journal on Multiscale and Multiphysics Computational Techniques, 5:5–18, 2019.

[16] Guokai Xu, Shaoqiu Xiao, Yan Li, and Bing-Zhong Wang. Modeling of electromagnetic radiation-induced from a magnetostrictive/piezoelectric laminated composite. Physics Letters A, 385:126959, 2021.

[17] Greg P Carman and Milan Mitrovic. Nonlinear constitutive relations for magnetostrictive materials with applications to 1-d problems. Journal of intelligent material systems and structures, 6(5):673–683, 1995.

[18] Yongping Wan, Daining Fang, and Keh-Chih Hwang. Non-linear constitutive relations for magnetostrictive materials. International Journal of Non-Linear Mechanics, 38(7):1053–1065, 2003.

[19] Mohsen Zaeimbashi, Mehdi Nasrollahpour, Adam Khalifa, Anthony Romano, Xianfeng Liang, Huaihao Chen, Neville Sun, Alexei Matyushov, Hwaider Lin, Cunzheng Dong, et al. Ultra-compact dual-band smart nems magnetoelectric antennas for simultaneous wireless energy harvesting and magnetic field sensing. Nature communications, 12(1):1–11, 2021.

[20] Ali Khaleghi, Reza Noormohammadi, and Ilangko Balasingham. Conductive impulse for wireless communication in dual-chamber leadless pacemakers. IEEE Transactions on Microwave Theory and Techniques, 69(1):443–451, 2020.

[21] Tahir Khaleeq, Harutomo Hasegawa, Michael Samuel, and Keyoumars Ashkan. Fixed-life or rechargeable battery for deep brain stimulation: which do patients prefer? Neuromodulation: Technology at the Neural Interface, 22(4):489–492, 2019.

[22] Carol L Baumbauer, Matthew G Anderson, Jonathan Ting, Akshay Sreekumar, Jan M Rabaey, Ana C Arias, and Arno Thielens. Printed, flexible, compact uhf-rfid sensor tags enabled by hybrid electronics. Scientific reports, 10(1):1–12, 2020.

[23] Takurō Ikeda. Fundamentals of piezoelectricity. Oxford university press, 1996.

[24] C Balanis. Antenna theory: analysis and design john wiley. Inc., Publication, 2005.

[25] Sami Gabriel, RW Lau, and Camelia Gabriel. The dielectric properties of biological tissues: Ii. measurements in the frequency range 10 hz to 20 ghz. Physics in medicine & biology, 41(11):2251, 1996.

[26] A Khaleghi and I Balasingham. Capacitively coupled electrode antenna: A practical solution for biomedical implants. In 2021 15th European Conference on Antennas and Propagation (EuCAP), pages 1–5. IEEE, 2021.